

Aggregation and disaggregation of senile plaques in Alzheimer disease

L. CRUZ*, B. URBANC*, S. V. BULDYREV*, R. CHRISTIE†, T. GÓMEZ-ISLA†, S. HAVLIN‡, M. MCNAMARA†, H. E. STANLEY*§, AND B. T. HYMAN†

*Center for Polymer Studies and Department of Physics, Boston University, Boston, MA 02215; †Neurology Service, Massachusetts General Hospital, Boston, MA 02114; and ‡Gonda-Goldschmid Center and Department of Physics, Bar-Ilan University, Ramat-Gan, 52900 Israel

Communicated by Herman Z. Cummins, City College of the City University of New York, New York, NY, May 7, 1997 (received for review March 14, 1997)

ABSTRACT We quantitatively analyzed, using laser scanning confocal microscopy, the three-dimensional structure of individual senile plaques in Alzheimer disease. We carried out the quantitative analysis using statistical methods to gain insights about the processes that govern $A\beta$ peptide deposition. Our results show that plaques are complex porous structures with characteristic pore sizes. We interpret plaque morphology in the context of a new dynamical model based on competing aggregation and disaggregation processes in kinetic steady-state equilibrium with an additional diffusion process allowing $A\beta$ deposits to diffuse over the surface of plaques.

Although the mechanism whereby $A\beta$ deposition may lead to dementia in Alzheimer disease (AD) is unknown, compelling genetic evidence suggests that aggregation of $A\beta$ to form senile plaques (SP) is an essential component of AD pathophysiology (1–3). Biochemical studies suggest that these $A\beta$ deposits are insoluble, and their formation process is viewed as irreversible. From inspection of AD tissue samples, it is evident that a wide variety of morphologies and textures of SP are present in the AD brain. Their morphologies cannot be explained by known aggregation models (4–8).

$A\beta$ is a ≈ 39 - to 42-amino acid amphipathic peptide derived from a portion of the transmembrane domain and extracellular region of the $A\beta$ precursor protein (9). $A\beta$ is a normal cellular product and is present in nanomolar concentrations in biological fluids (10, 11). *In vitro*, at higher concentrations, it is extremely insoluble and precipitates to form aggregates (12–15). In the AD brain, $A\beta$ deposits form β -pleated, sheets which are the major constituent of SP. Racemized amino acids have been found in $A\beta$, suggesting that at least some of the deposits are long-lived (16). Given the insoluble nature of $A\beta$, it is reasonable to predict that plaques would continue to grow in size and number as the disease progresses. However, experimental data show that this is not the case; instead, plaque size and $A\beta$ burden (total percentage) appear to remain relatively constant over a wide range of disease durations (17–19).

Optical microscopy of the AD brain reveals innumerable $A\beta$ deposits of various sizes and shapes. In an effort to understand how $A\beta$ deposition occurs and evolves over time, we have examined the fine structure of the SP using confocal scanning laser microscopy (20, 21) and immunofluorescence techniques for $A\beta$ immunostaining. The confocal microscope is able to obtain optical sections that are ≈ 0.3 - to 0.5 - μm thick, allowing the reconstruction of the three-dimensional fine structure of a plaque with a resolution close to the theoretical limit of the order of the wavelength of visible light.

Standard immunostaining in thick sections might suggest that plaques are relatively solid (Fig. 1*a*), but our examination of individual cross-sections using confocal microscopy reveals cavities and inner structure, suggesting that the three-dimensional structure of $A\beta$ aggregates in SPs is porous [Fig. 1*b*]. By stepping through the $A\beta$ deposit in a chosen direction, sequential optical sections similar to those shown in Fig. 1*c* can be obtained and reconstructed to analyze the three-dimensional structure of the plaque (Fig. 1*d*).

The first approach to quantify the geometry of these individual plaques is to calculate the density–density correlation function (22) $g(r)$, which is defined to be the probability that two points of space at a distance r are both part of the SP. Results from cross-sections of typical cortical samples (Fig. 3*a*) indicate that, in contrast to that of a solid disk (shown by a solid line), the correlation function displays three regimes: (i) a central region that approximates the solid disk curve and (ii) an inner and (iii) an outer regime that deviate. The deviations from the solid line in the small r regime indicate the existence of “pockets” of higher and lower density than the average density, corroborating the conclusion derived by simple inspection of confocal pictures (Fig. 1*b* and *c*). For larger distances, the deviation indicates that the density of the plaque decays slowly (diffuse ring) as the distance from the center of the plaque increases.

To further study the characteristics of the inner structure of the plaques and thus gain some insight into the formation of SP, we performed the correlation function analysis again, but now exclusively over the cross-sectional area of the plaque confined to its interior. In this way, there are no surface effects on the calculation, so this analysis yields information only about the plaque’s inner structure. Over 500 images were collected; correlation function analysis of middle sections of plaques of diameters ranging from 20 to 90 μm (Fig. 3*b*) indicated that the average linear size of these pores or “pockets” of different density is, at most, only weakly diameter-dependent, being roughly 5 ± 2 μm (see the *Inset* of Fig. 3*b*). Double immunostaining using 4', 6-diamidino-2-phenylindole for nuclei, LN-3 for microglia, or glial fibrillary acidic protein for astrocytes showed that these pores are infrequently occupied by cellular elements.

Thus, these quantitative analyses of plaque structure revealed two new features not evident by qualitative inspection. A typical plaque consists of (i) a porous core with pores of a characteristic size and (ii) a diffuse ring whose density slowly decays from the center of mass of the SP. Recognition of these two features immediately leads to the question of how these structures are formed in the AD brain and what kind of mechanisms could produce such morphologies. Consideration of general principles of aggregation leads to several possibil-

The publication costs of this article were defrayed in part by page charge payment. This article must therefore be hereby marked “advertisement” in accordance with 18 U.S.C. §1734 solely to indicate this fact.

© 1997 by The National Academy of Sciences 0027-8424/97/947612-5\$2.00/0
PNAS is available online at <http://www.pnas.org>.

Abbreviations: SP, senile plaques; AD, Alzheimer disease.

§To whom reprint requests should be addressed. e-mail: hes@buphyk.bu.edu.

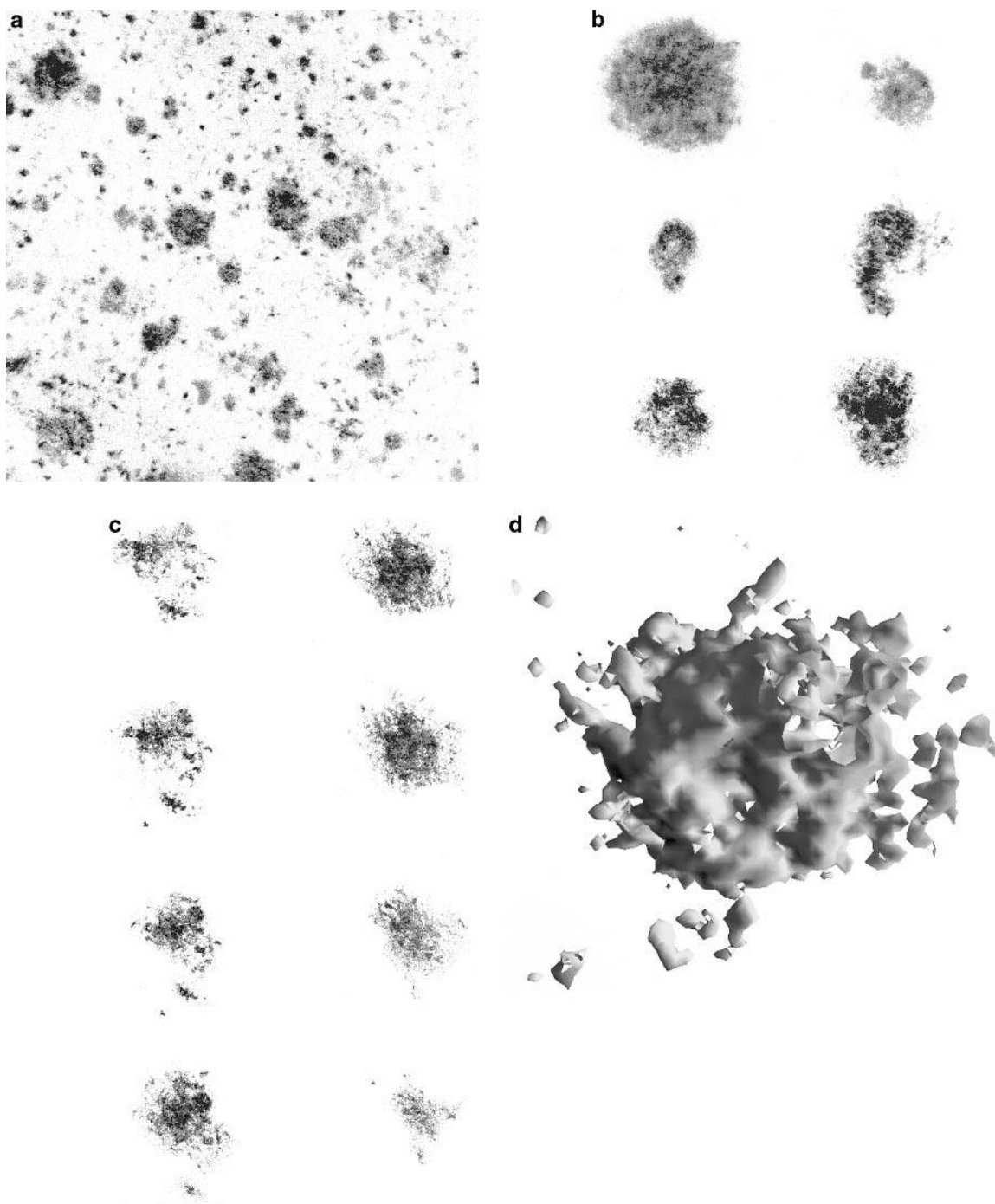


FIG. 1. (a) Photomicrograph from a Bio-Rad 1024 confocal microscope of a section of cerebral tissue of dimensions $600 \times 600 \mu\text{m}$ in area, displaying plaque aggregates as dark regions. Immunofluorescence used anti- $A\beta$ mAb 10D5 on $50\text{-}\mu\text{m}$ thick frozen sections as described (17). Immunoreactivity was visualized using a Cy-5-labeled secondary antibody (Jackson ImmunoResearch) to overcome potential problems due to tissue autofluorescence. Qualitative analysis of the figure shows that the $A\beta$ aggregates are of roughly spherical shape. Quantitative analysis shows that the size distributions are peaked around a characteristic size. (b) Typical plaques and (c) consecutive cross-sections of an individual plaque, as observed under a confocal microscope, are shown. (d) Three-dimensional reconstruction of an SP (of diameter $\approx 60 \mu\text{m}$) from 18 images ($\times 100$ oil immersion objective) separated by $0.3 \mu\text{m}$. Each cross-sectional image represents the average of three scans combined with a Kalman filter. All images were obtained from the multimodal superior temporal sulcus neocortex of six Alzheimer cases from the Massachusetts Alzheimer Disease Research Center Brain Bank.

ities that depend on the diffusion constant of $A\beta$ (4–8, 22–26). If the diffusion of the solute $A\beta$ is slower than the speed of aggregation, the growth will occur at the tips of the aggregate, leading to a ramified tree-like structure belonging to the diffusion limited aggregation universality class (5–8, 22–26) rather than the structure observed. This case is very unlikely to occur in AD brains because, it is believed, aggregation is a slow process that may continue for years while the diffusion of

$A\beta$ in the brain is much faster. On the other hand, if the diffusion of $A\beta$ is faster than the aggregation, then $A\beta$ is equally likely to aggregate at any point on the surface of the SP. The outcome is a very compact spherical structure with only a few very small pores, belonging to the Eden universality class (5–8, 22–26), which is also quite different than the experimentally observed morphology. Physicochemical models based on nucleation-dependent polymerization, as sug-

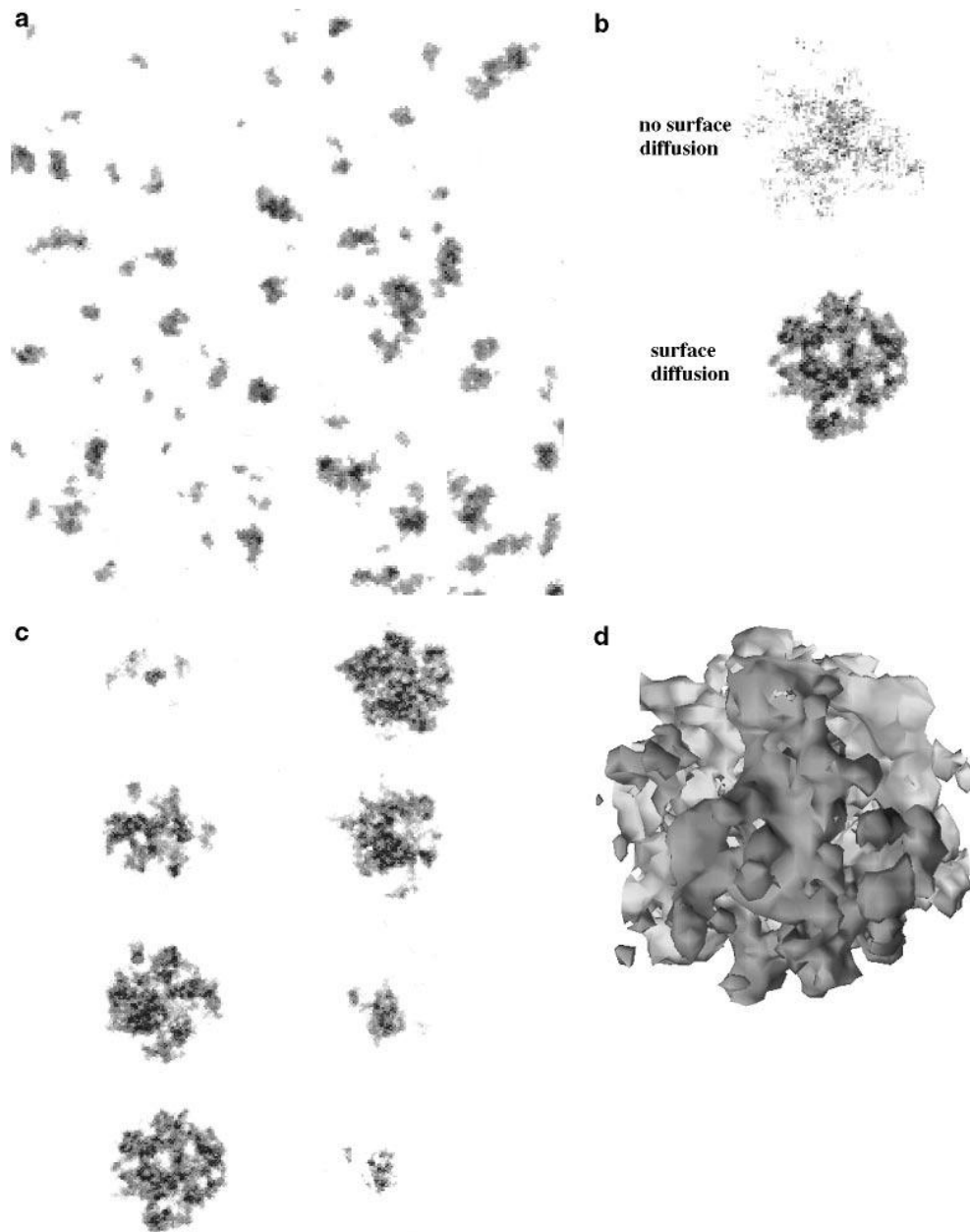


FIG. 2. The dynamical model is defined on a discrete three-dimensional lattice with lattice sites that can be either empty or occupied. At each time step in the simulation, each occupied site either grows with probability P_g or is cleared with probability P_c . Depending on the relative values, a system may be predisposed to create plaques or to dissolve them. Nearest neighbor rules are incorporated such that aggregation at a site is more likely if its neighboring sites are empty and less likely if they are occupied. On the other hand, an occupied site is more likely to be dissolved as the number of empty nearest sites increases. These rules follow from considering that, in real SP, the more exposed sites have a greater probability of being surrounded by $A\beta$. At the same time, these exposed sites are more likely to be disaggregated by external agents. To avoid the final state in which either all sites are occupied or empty (inevitable under the given rules), it is necessary to incorporate a dynamic feedback that allows the system to evolve into a steady state characterized by a burden that is, on average, conserved in time. The feedback modifies P_c by an amount that is proportional to the rate of change in the total burden. In addition, the model allows for a diffusion of aggregated particles on the model plaque. This diffusion permits a given occupied site to explore its immediate neighborhood and choose to change its position only if it ends up surrounded by more neighboring sites. This selective diffusive process allows for the system to relax so that the overall surface is smooth. In *a*, a cross-section of a system defined on a three-dimensional lattice of the size $400 \times 400 \times 20$ after 500 time steps. The initial configuration corresponds to randomly scattered seeds covering 2% of the lattice sites. The initial values of the disaggregation and aggregation probabilities are $P_c = P_g = 0.8$. The surface diffusion is set to allow sites to move up to 10 steps around its initial position at every time step. (*b*) Typical cross-sections of two model plaques (of diameter ≈ 50 pixels) after 500 time steps, illustrating the effect of surface diffusion. The initial value of the disaggregation and growth probabilities are the same as in *a*. Starting with a small solid sphere as an initial condition, the model with no surface diffusion evolves into a too diffuse object with less well defined pores when compared with the lower one, which is a result of the model with diffusion. *c* and *d* show eight consecutive two-dimensional cross-sections and three-dimensional reconstruction of the model plaque from *b*, respectively.

gested by Jarrett and Lansbury (27), would yield a compact object if the process is continued beyond the nucleation and growth steps.

We suggest an alternative possibility in which aggregation occurs simultaneously with disaggregation. Objects grown by

our proposed process can lead to the formation of porous objects whose size distributions, number, and $A\beta$ burden are constant if the aggregation is in dynamic equilibrium with disaggregation (17). Our hypothesis is not inconsistent with the nucleation process proposed by Jarrett and Lansbury (27), but

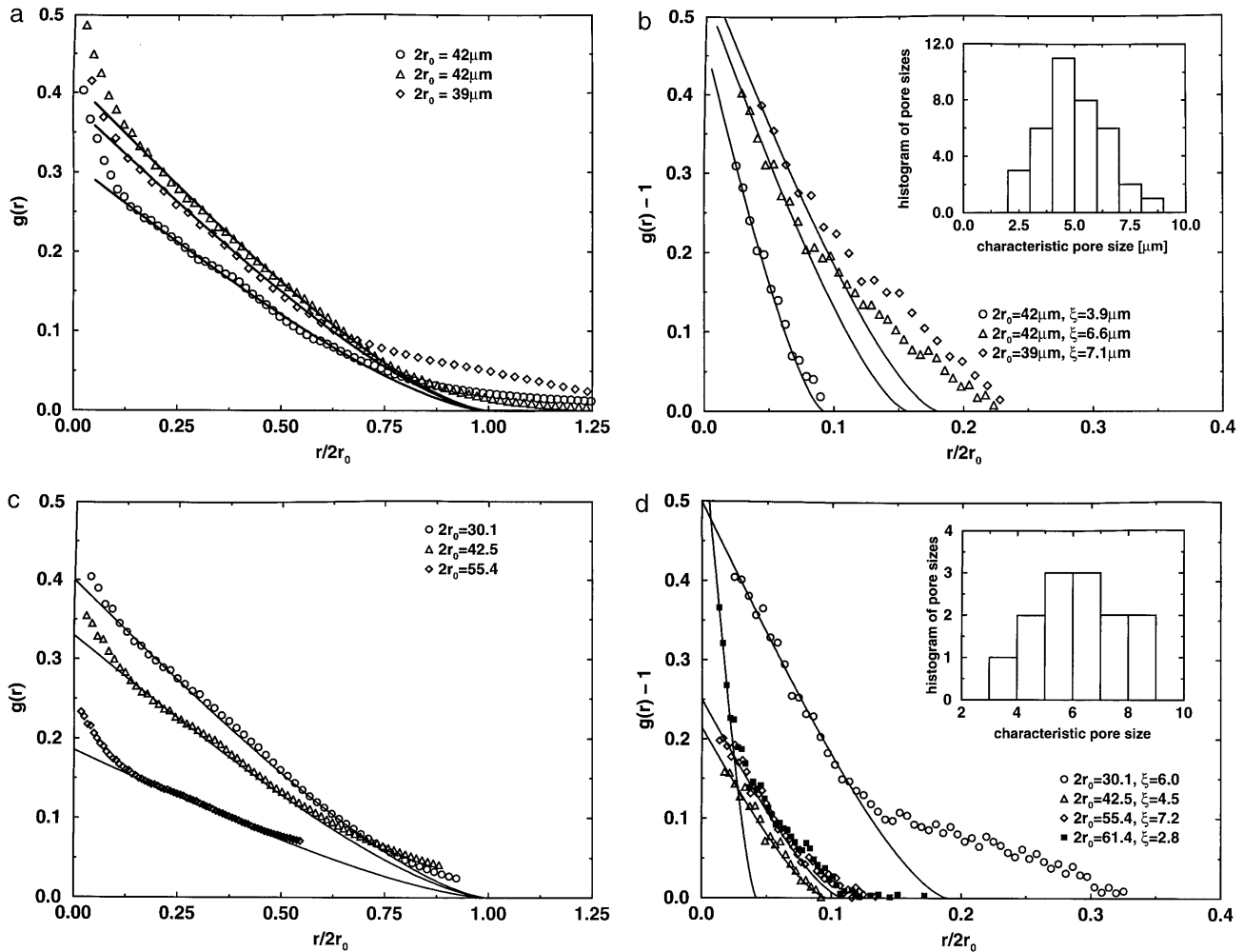


FIG. 3. Correlation functions calculated for the cross-sections of over 500 images representing 37 plaques from the superficial layers of the superior temporal sulcus cortex in tissue of Alzheimer brain (*a* and *b*) and for the cross-sections of computer-simulated model plaques (*c* and *d*). Plaques from tissue were not selected to represent any morphological subtype. In fact, it is difficult to categorize with certainty the three-dimensional confocal images of $A\beta$ deposits into “classic,” “cored,” or “primitive” plaques. In *a*, the calculation considers the plaque and its surroundings. In *b*, only the interior region of a plaque is considered in the correlation function calculation. Our choice of normalization in the correlation function is such that, as $r \rightarrow \infty$, the correlation function tends to the normalized density of the system [$g(\infty) = 0$ in *a* and $= 1$ in *b*]. The parameter r_0 for each graph indicates the characteristic radius of the entire plaque and is obtained from the solid disk fit. The characteristic size, ξ , of the porosity inside plaques is obtained from the x -axis intercept of the small- r fits to a solid disk of $g(r)$ calculated as in *b*. The fit is carried out exclusively over the small- r region because we were interested in the smallest homogeneous structure inside the plaque. The *Inset* in *b* shows a histogram of pore sizes from plaques that peaks at $\approx 5 \mu\text{m}$ (much larger than the resolution of the images). (*c*) Correlation function for the computer-simulated model plaques taking into account the model plaque with the surroundings and (*d*) taking into account only the interior of the model plaque. In both *c* and *d*, the solid lines are fits to a correlation function of a solid disk. The *Inset* in *d* shows a histogram of pore sizes in cross-sections of 13 different model plaques of different diameters. The histogram shows a peak at a characteristic pore size of ≈ 6 pixels. The curve in *d* with the black squares is the interior correlation function for the model plaque without surface relaxation (top of Fig. 2*b*), giving a considerably smaller value than that for the model with surface relaxation.

extends it by adding a disaggregation process that, once the thermodynamic equilibrium is reached, would yield a porous structure similar to that found experimentally. This also does not preclude the possibility that, in addition to a dynamic equilibrium between soluble and deposited $A\beta$, some $A\beta$ undergo irreversible biochemical changes to long-lived species (16).

To corroborate the expected outcomes from these hypothesized competing aggregation and disaggregation mechanisms, we developed a dynamical model. The model incorporates the experimental observation that the amount of $A\beta$ burden varies within a narrow range and is independent of duration or severity of illness (28). In the model, an ensemble of plaques, as well as individual plaques of various sizes, are grown on a three-dimensional lattice. A collection of model plaques, grown in a computer simulation starting from a configuration of isolated occupied lattice points, is shown in Fig. 2*a* (to be

compared with actual plaques shown in Fig. 1*a*). The size distribution of configurations of model plaques, like the one represented in Fig. 2*a*, was found to exhibit a peaked distribution—in agreement with earlier experimental work (28). The two computer-generated model plaques presented in Fig. 2*b* show the importance of the inclusion of surface diffusion in the model, which allows the model plaques to acquire a smoother surface (note the difference between the two model plaques in Fig. 2*b*). In addition, as a consequence of the surface diffusion, the model exhibits well defined pores in its interior (lower model plaque in Fig. 2*b*). Fig. 2*c* and *d* shows cross-sections and three-dimensional reconstruction of a typical model plaque, respectively (compare with Fig. 1*c* and *d*). To make quantitative comparisons between the experiment and the model, in Fig. 3*c* and *d* we present results for the correlation function of the model plaques. Similarly to Fig. 3*a*, Fig. 3*c* exhibits a porous core and diffuse ring around the core

for the model plaques. Comparing the *Insets* of Fig. 3 *b* and *d*, we concluded that the model was able to reproduce the distribution of average pore and pocket sizes in the cross-sections of SPs.

In summary, using laser scanning confocal microscopy, we were able to obtain three-dimensional images of SP. Using correlation function analysis, we examined the fine structure of SPs, and we have discovered within the plaque's internal morphological structure the presence of characteristic size pores and pockets of higher density (Figs. 1 and 3*b*). This structure serves to decrease the likelihood of several potential formation mechanisms based solely on aggregation and favors instead a model in which both aggregation and disaggregation processes are in dynamic steady-state equilibrium. The requirement of a disaggregation mechanism in the model is consistent with the possibility that $A\beta$ deposition may not be irreversible. The plausibility of this model is further supported by (i) analyses of a small number of patients studied at both biopsy and autopsy, in whom a decrease (or no increase) in $A\beta$ deposits was seen (29, 30), and (ii) *in vitro* studies suggesting that microglia can respond to and ingest $A\beta$ aggregates (31, 32).

We thank D. Futer and R. Mantegna for very helpful discussions. This work was supported by National Institutes of Health Grant AG08487 and by generous gifts from the Walters Family Foundation. We also thank the Massachusetts Alzheimer Disease Research Center Brain Bank (National Institute on Aging Grant AG05134; Dr. E. T. Hedley-Whyte, director) for tissue samples.

1. Selkoe, D. (1994) *J. Neuropathol. Exp. Neurol.* **53**, 438–447.
2. Goate, A., Chartier-Harlin, M.-C. & Mullan, M. (1991) *Nature (London)* **349**, 704–707.
3. Cai, X.-D., Golde, T. E. & Younkin, S. G. (1993) *Science* **259**, 514–516.
4. de Gennes, P.-G. (1979) *Scaling Concepts in Polymer Physics* (Cornell Univ. Press, Ithaca, NY).
5. Family, F. & Landau, D. P., eds. (1984) *Kinetics of Aggregation and Gelation* (Elsevier, Amsterdam).
6. Herrmann, H. J. (1986) *Physiol. Rep.* **136**, 153–227.
7. Vicsek, T., Shlesinger, M. F. & Matsushita, M., eds. (1994) *Fractals in Natural Sciences* (World Scientific, Singapore).
8. Grosberg, A. Y. & Khokhlov, A. R. (1994) *Statistical Physics of Macromolecules* (Am. Inst. Physics, New York).
9. Lansbury, P. T., Jr. (1992) *Biochemistry* **31**, 6865–6870.
10. Seubert, P., Vigo-Pelfrey, C., Esch, F., Lee, M., Dovey, H., Davis, D., Sinha, S., Schlossmacher, M., Whaley, J., Swindlehurst, C., McCormack, R., Wolfert, R., Selkoe, D., Lieberburg, I. & Schenk, D. (1992) *Nature (London)* **359**, 325–327.
11. Shoji, M., Golde, T. E., Ghiso, J., Cheung, T. T., Estus, S., Shaffer, L. M., Cai, X.-D., McKay, D. M., Tintner, R., Frangione, B. & Younkin, S. G. (1992) *Science* **258**, 126–129.
12. Lomakin, A., Chung, D. S., Benedek, G. B., Kirschner, D. A. & Teplow, D. B. (1996) *Proc. Natl. Acad. Sci. USA* **93**, 1125–1129.
13. Fraser, P. E., Nguyen, J. T., Inouye, H., Surewicz, W. K., Selkoe, D. J., Podlisny, M. B. & Kirschner, D. A. (1992) *Biochemistry* **31**, 10716–10723.
14. Barrow, C. J., Yasuda, A., Kenny, P. T. M. & Zagorski, M. G. (1993) *J. Mol. Biol.* **225**, 1075–1093.
15. Pike, C. J., Burdick, D., Walencewicz, A. J., Glabe, C. G. & Cotman, C. W. (1993) *J. Neurosci.* **13**, 1676–1687.
16. Shapira, R., Austin, G. E. & Mirra, S. S. (1988) *J. Neurochem.* **50**, 69–74.
17. Hyman, B. T., Marzloff, K. & Arriagada, P. V. (1993) *J. Neuro-pathol. Exp. Neurol.* **52**, 594–600.
18. Arriagada, P. V., Growdon, J. H., Hedley-Whyte, E. T. & Hyman, B. T. (1992) *Neurology* **42**, 631–639.
19. Berg, L., McKeel, D. W., Miller, J. P., Baty, J. & Morris, J. C. (1993) *Arch. Neurol.* **50**, 349–358.
20. Lichtman, J. W. (1994) *Sci. Am.* **271**(8), 40–45.
21. Wilson, T., ed. (1990) *Confocal Microscopy* (Academic, New York).
22. Vicsek, T. (1992) *Fractal Growth Phenomena* (World Scientific, New York), 2nd Ed.
23. Avnir, D., ed. (1989) *The Fractal Approach to Heterogeneous Chemistry* (Wiley, Chichester).
24. Takayasu, H. (1990) *Fractals in the Physical Sciences* (Manchester Univ. Press, Manchester, U.K.).
25. Bassingthwaite, J. B., Liebovitch, L. S. & West, B. J. (1994) *Fractal Physiology* (Oxford Univ. Press, New York).
26. Stanley, H. E. & Ostrowsky, N., eds. (1985) *On Growth and Form: Fractal and Nonfractal Patterns in Physics* (Martinus Nijhoff, Dordrecht, The Netherlands).
27. Jarrett J. T. & Lansbury, P. T. (1993) *Cell* **73**, 1055–1058.
28. Hyman, B. T., West, H. L., Rebeck, G. W., Buldyrev, S. V., Mantegna, R. N., Ukleja, M., Havlin, S. & Stanley, H. E. (1995) *Proc. Natl. Acad. Sci. USA* **92**, 3586–3590.
29. Mann, D. M. A., Marcyniuk, B., Yates, P. O., Neary, D. & Snowden, J. S. (1988) *Neuropathol. Appl. Neurobiol.* **14**, 177–195.
30. Gearing, M., Schneider, J. A., Mori, H. & Mirra, S. S. (1996) *J. Neuropathol. Exp. Neurol.* **55**, 645.
31. Paresce, D., Ghosh, R. & Maxfield, F. R. (1996) *Neuron* **17**, 553–565.
32. El-Khoury, J. (1996) *Nature (London)* **382**, 716–719.